**Mediterranean Marine Science**

Vol 21, No 2 (2020)

Vol 21, n2


# One-year assessment of the CHAOS two-way coupled atmosphere-ocean wave modelling system over the Mediterranean and Black Seas

*GEORGE VARLAS, CHRISTOS SPYROU, ANASTASIOS PAPADOPOULOS, GERASIMOS KORRES, PETROS KATSAFADOS*

doi: 10.12681/mms.21344

Research Article

*Mediterranean Marine Science*
Indexed in WoS (Web of Science, ISI Thomson) and SCOPUS
The journal is available on line at http://www.medit-mar-sc.net
DOI: http://dx.doi.org/10.12681/mms.21344

# One-year assessment of the CHAOS two-way coupled atmosphere-ocean wave modelling system over the Mediterranean and Black Seas

**George VARLAS[1,2], Christos SPYROU[2], Anastasios PAPADOPOULOS[1], Gerasimos KORRES[3] and Petros KATSAFADOS[2]**

[1] Institute of Marine Biological Resources and Inland Waters, Hellenic Centre for Marine Research (HCMR), 46.7 Km Athens-Sounion Avenue, 19013 Anavyssos, Attica, Greece
[2] Department of Geography, Harokopio University of Athens (HUA), El. Venizelou Str. 70, 17671 Athens, Greece
[3] Institute of Oceanography, HCMR, 46.7 Km Athens-Sounion Avenue, 19013 Anavyssos, Attica, Greece

Corresponding author: pkatsaf@hua.gr

Handling Editor: Christos ARVANITIDIS; Stelios SOMARAKIS

Received: 26 September 2019; Accepted: 15 March 2020; Published on line: 22 June 2020

## Abstract

It is currently clear that the atmosphere and ocean should be simulated by integrated modelling systems resolving interconnected physical factors that determine the Earth's energy balance. Waves play a key role in the interfacial interaction between the atmosphere and the ocean, regulating momentum, heat and moisture exchange. This study aims to evaluate the CHAOS two-way coupled atmosphere-ocean wave system (Chemical Hydrological Atmospheric Ocean wave System) over the Mediterranean and Black Seas. The evaluation is performed against in situ and remote sensing data for the period from 1 December 2013 to 1 December 2014. CHAOS includes the Weather Research Forecasting (WRF) model, version 3.8, as atmospheric component and the Wave model (WAM) cycle 4.5.4 as ocean wave component, coupled through the OASIS3-MCT coupler, version 3.0. Two continuous model simulation approaches were followed to assess the impact of atmosphere-ocean waves coupling. In the first approach (1-way coupling mode), the ocean wave component uses the winds produced by the atmospheric component, while in the second approach (2-way coupling mode) the atmospheric component additionally uses sea state information estimated by the ocean wave component through wave-dependent Charnock parameter computations. In the 2-way coupling mode, the attenuation of the atmospheric flow has a damping effect on wind-generated waves. The simulations in 2-way coupling mode produce more realistic results yielding statistical improvements. Compared against buoy observations, the 2-way mode reduces the root mean square error (RMSE) 1.2% for wind speed and 6.3% for significant wave height, while against Jason-2 satellite retrievals the reduction is 0.5% and 2.4%, respectively. Additionally, the 2-way coupling mode outperformed the 1-way mode under intense wind and wave conditions during the one-year period considered.

**Keywords:** Air-sea interaction; WRF; WAM; sea surface roughness; wind-wave coupling; statistical evaluation.

## Introduction

The importance of dynamic and thermodynamic exchanges between the ocean and the atmosphere has been underlined in several studies throughout the years. Mass exchange in the air-sea interface is accompanied by latent heat transfer, e.g. along the coastal zone and in semi-enclosed basins such as the Mediterranean Sea, while the dynamic interaction between the atmosphere and waves determines sea surface aerodynamic roughness, which in turn affects momentum, heat and moisture exchanges (Black *et al.,* 2007; Drennan *et al.*, 2007; French *et al.*, 2007; Zhang *et al.,* 2008; Andreas, 2011; Bell *et al.,* 2012; Katsafados *et al.,* 2016, 2017, 2018; Wahle *et al.,* 2017; Varlas *et al.,* 2018). Therefore, air-sea exchanges depend on properties such as wind speed, surface roughness, water vapour, currents, temperature, salinity etc (Breivik *et al.,* 2015; Carniel *et al.,* 2016; Ličer *et al.,* 2016; Staneva *et al.,* 2016; Bonaldo *et al.,* 2019). Atmosphere-wave interaction determines sea surface roughness and near surface wind speed, modifying the transfer of kinetic energy and enthalpy (Doyle, 1995; Bao *et al.,* 2000; Fairall *et al.,* 2003) as well as sea spray that plays a crucial role in heat exchange (Rizza *et al.,* 2018). More specifically, winds near the surface of the ocean, along with medium to high frequency gravity waves, are the main precursors of sea surface roughness, which impact the momentum and energy exchange between the ocean and the atmosphere (Janssen, 1989, 1991; Donelan *et al.,* 2004; Varlas *et al.,* 2018). High-frequency wind-generated waves increase

sea surface roughness and drain energy and momentum from the atmosphere (Rutgersson *et al.,* 2012; Katsafados *et al.,* 2016; Wahle *et al.,* 2017). Sea surface roughness in turn controls the latent and sensible heat fluxes as well as water transfer between the atmosphere and the ocean (Bruneau & Toumi, 2016; Carniel *et al.,* 2016; Ricchi *et al.,* 2017). These modifications affect the physical processes of the atmospheric boundary layer (Sullivan *et al.,* 2008; Jenkins *et al.,* 2012; Varlas *et al*., 2018).

Several studies have also shown the relevance of the sea state dependent momentum transfer for storm-surge modelling (Sikirić *et al.,* 2013), ocean circulation modelling (Benetazzo *et al.,* 2014; Breivik *et al.,* 2015; Carniel *et al.,* 2016; Ličer *et al.,* 2016; Ricchi *et al.,* 2017), weather prediction (Katsafados *et al.,* 2016; Wahle *et al.*, 2017; Varlas *et al.,* 2018) and atmospheric climate (e.g. Voldoire *et al.,* 2013). Air-sea momentum and heat exchange play a crucial role in the development of cyclones, which are associated with extreme winds, torrential rainfall, high waves and damaging storm surges leading to extensive coastal flooding thus inflicting human casualties and economic damages in the affected areas (Varlas, 2017; Varlas *et al*., 2018; Katsafados *et al*., 2018; Varlas *et al*., 2019c; Strajnar *et al.,* 2019).

A deeper understanding of air-sea interactions is of great importance for life on earth and human activities. Therefore, it becomes vital to reliably predict the genesis and life cycle of extreme weather phenomena and the associated air-sea interaction (Ricchi *et al.,* 2019). This necessity led to the development of multi-model and multi-scale advanced numerical systems that can simulate the atmospheric and oceanic processes in a coupled way (Hodur, 1997; Janssen *et al.,* 2002; Chen *et al.,* 2013; Varlas *et al*., 2018 and others). These models help the scientific community to understand the details of air-sea interactions and study the feedback generated by such phenomena in both mediums (air and water). Beyond the scientific merits, such a system is expected to offer better wind and wave forecasts, which are related to wind and wave power production (Christakos *et al.,* 2016), and provide early warnings of extreme phenomena (Christakos *et al.,* 2014). Moreover, improved wind and wave forecasts are expected to facilitate all human activities associated with the sea such as marine transportation (Tucker & Pitt, 2001), oil extraction, fisheries, tourism and coastal constructions.

In order for a coupled system to provide accurate and reliable forecasts, it needs to be calibrated and evaluated for an adequate period of time. To this end, a state-of-the-art atmosphere-ocean wave modelling system, namely CHAOS (Chemical Hydrological Atmospheric Ocean wave System; Varlas, 2017; Varlas *et al.,* 2018) has been applied across the Mediterranean and Black Seas for an extended period of time (one year) and evaluated with a significant number of in situ and remote sensing data. Two sets of simulations are performed: one where the atmosphere does not consider ocean waves (1-way coupling mode) and another where sea state affects air processes (2-way coupling mode) through the modification of sea surface roughness. Both results are statistically evaluated against in situ measurements and remote sensing estimates. The rest of the manuscript is organized as follows:

Section 2 presents the configuration of the modelling system and the one-year design of the simulations. Section 3 describes the data and methodology used for the statistical assessment. The simulation results for the 1-way and 2-way coupling modes are evaluated and discussed in Section 4. Finally, the main conclusions of this study are presented in Section 5.

## Experimental Setup

CHAOS consists of the Weather Research Forecasting (WRF) model, version 3.8 (Skamarock *et al.,* 2008; Powers *et al*., 2017) as atmospheric component and the Wave model (WAM) cycle 4.5.4 (WAMDI, 1988; Komen *et al.,* 1994) as ocean wave component, coupled through the OASIS3-MCT coupler version 3.0 (Valcke *et al.,* 2015) (Fig. 1). CHAOS also includes the WRF-Hydro version 3.0 (Gochis *et al.,* 2015) and WRF-Chem version 3.8 (Grell *et al.,* 2005) models to represent hydrological and chemical processes, respectively, when needed, e.g. for flash flood simulations (Varlas *et al.,* 2019a). The hydrological and chemical components of CHAOS are not activated in this study.

Two configurations of CHAOS have been applied to perform the simulations (Varlas, 2017; Varlas *et al.,* 2018):

- 2-way coupling mode (2-way): The ocean wave component uses the u and v components of wind at 10 meters produced by the atmospheric component. Meanwhile, the atmospheric component uses sea state information to estimate roughness length (Eq. 1) through the wave-dependent Charnock parameter estimated by the ocean wave component, employing Janssen's parameterization scheme (Janssen, 1989, 1991; Eq. 2).

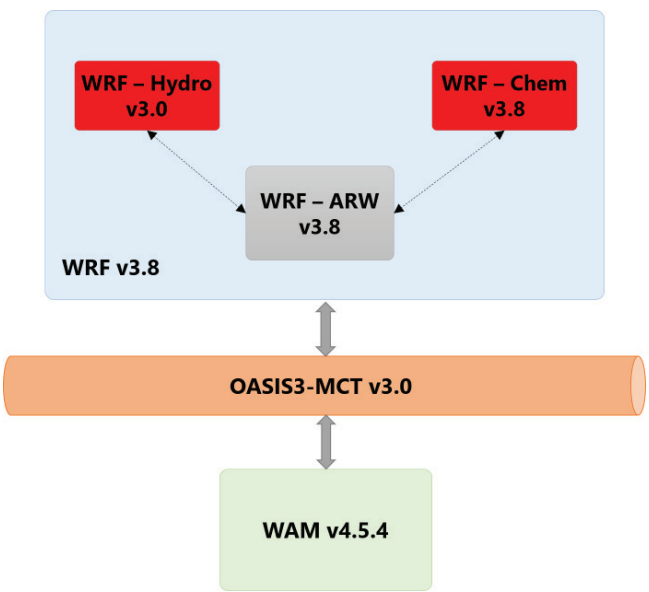


***Fig. 1:*** The components of CHAOS (Varlas, 2017; Varlas *et al.,* 2018). WRF-Hydro and WRF-Chem (depicted with red colour) are not activated in this study.

- 1-way coupling mode (1-way): The ocean wave component uses the u and v components of wind at 10 meters produced by the atmospheric component. The Charnock parameter in the atmospheric component remains constant and equal to 0.0185 (Wu, 1982) throughout the simulations. The results of this simulation mode are used as a reference for the sensitivity tests and the statistical evaluation of the 2-way coupling mode.

The roughness length $z_0$ is estimated by the atmospheric component through Eq. (1):

$$z_0 = \frac{au_*^2}{g} + \frac{0.11v}{u_*}$$

where $g$ is gravitational acceleration, $u_*$ is friction velocity, $v$ is air kinematic viscosity and $a$ is the Charnock parameter. The wave-dependent Charnock parameter is estimated by the ocean wave component, according to Janssen's (1989, 1991) quasi-linear theory of wind wave generation, through Eq. (2):

$$\alpha = \frac{0.01}{\sqrt{1 - \frac{\tau_w}{\tau}}}$$

where $\tau_w$ is wave stress and $\tau$ is total stress, which is defined as the sum of the wave stress and the turbulent stress neglecting the viscous stress (Janssen, 1989, 1991).

CHAOS has been configured to run on a domain covering the Mediterranean Sea and the Black Sea. The atmospheric component uses Arakawa semi-staggered C-grid in a horizontal resolution of 10 km x 10 km, a time step of 60 sec and 38 vertical levels stretching from the surface to 50 hPa (Fig. 2). Gridded analysis data from the European Centre for Medium-Range Weather Forecasts (ECMWF) in horizontal resolution of 0.5° x 0.5° and time increment of 6 hours were used for the creation of the initial and boundary conditions of the atmospheric component. Moreover, ECMWF Sea Surface Temperature (SST) analyses were used for SST update every 6 hours during the simulations. The Global Multi-resolution Terrain Elevation Data (30-arc-sec USGS GMTED 2010; Danielson & Gesch, 2011), vegetation data MODIS FPAR (Myneni *et al.,* 2002) and land-use data 21-class IGBP MODIS (Friedl *et al.,* 2010) were used as static input data in the pre-processing stage of the atmospheric component.

The revised Monin-Obukhov scheme (Jiménez *et al.,* 2012) is used to simulate the processes in the surface layer, involving several modifications to encapsulate sea state information (Varlas, 2017; Varlas *et al.,* 2018). For the simulation of Planetary Boundary Layer (PBL) processes, the Yonsei University scheme (Hong *et al.,* 2006; YSU) is used. The ground processes are simulated using the unified land surface model (Tewari *et al.,* 2004; Unified NOAH). In order to resolve the long-wave and short-wave radiation processes, the RRTM (Mlawer *et al.,* 1997) and the Dudhia (1989) schemes are employed, respectively. In order to simulate the microphysics and convective processes, the Thompson scheme (Thompson *et al.,* 2008) and the Kain-Fritsch scheme (Kain, 2004) are used, respectively.

The ocean wave component uses a spherical latitude-longitude grid. The grid of the wave model for the Mediterranean and Black seas covers the geographical area between 8° W - 42° E and 29° N - 48° N, as shown in Figure 2 (black line), with a horizontal resolution of 0.1° x 0.1°. WAM has a propagation time step of 75 sec and a source time step of 600 sec (10 min). WAM uses 24 directional bins (15° directional resolution) and 25 frequency bins (ranging from 0.042 to 0.411 Hz) to represent the wave spectra distribution. The initialization of WAM is based on the "hot start" approach in order to use realistic initial wave spectrum. The initial wave spectrum is computed by a pre-processing CHAOS simulation for a time period of one day before the initial time of each case

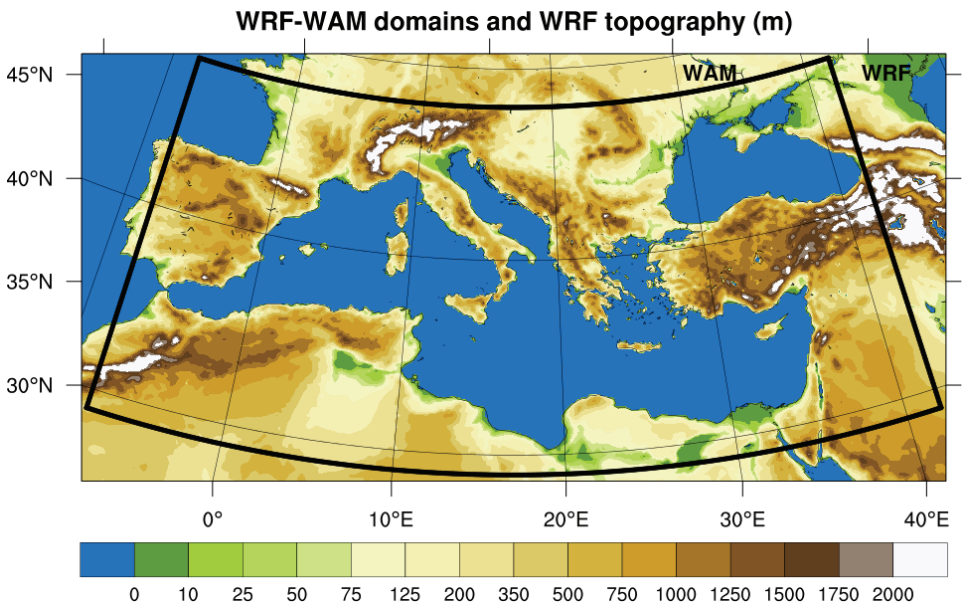


***Fig. 2:*** Domains of the WRF and WAM (black line) models, as components of CHAOS. The topography (m) used by the WRF model is also depicted. The topographic map has been constructed from the 30-arc-sec USGS GMTED 2010 dataset (Danielson & Gesch, 2011).

study. The bathymetric map has been constructed from Etopo1 data (Amante & Eakins, 2009; 1 min Gridded Global Relief Data) using bilinear interpolation (Fig. 3). Local corrections have been introduced in shallow areas of the Mediterranean and Black Sea basins. Additionally, a shallow water approximation with depth refraction and depth-induced wave breaking (Battjes & Janssen, 1978) is employed due to the complex bathymetry of the domain. The shallow water approximation includes the wave energy loss due to bottom friction and percolation and it is preferred for high resolution simulations (e.g. Korres *et al.,* 2011). Furthermore, as proposed by Katsafados *et al.* (2016), the Strait of Gibraltar, Dardanelles and Bosporus are considered as closed boundaries; thus, no wave energy is advected through these straits.

The different projections of the two components yield a mismatch between the two domains. Thus, a constant Charnock parameter is implemented for the sea grid points of the atmospheric domain (e.g. near its north-western boundaries), which are outside the WAM model domain. The constant value 0.0185 (Wu, 1982) for the Charnock parameter is widely applied in uncoupled and 1-way coupled simulations (Varlas, 2017). A 1-2-1 smoothing filter with weights of 1, 2, and 1 for the grid points (i-1,j), (i,j), and (i+1,j) is also applied in the transition zone, from outside to inside the WAM domain in the Atlantic Ocean, in order to eliminate artificially-generated waves. Moreover, the initial input sea state parameters in WRF were calculated by the pre-processing 1-day WAM simulation to obtain more realistic initial sea state conditions. Each component of CHAOS maintains its own time step. Thus, the coupling procedure exchanges data on the source time step of the WAM model, every 600 seconds. As the time step of the atmospheric model is 60 sec, the exchange takes place every 10 time steps of the atmospheric model. The configuration of the system and the main parameterization schemes used are summarized in Table 1.

The execution of the continuous simulations is designed using an operational approach, based on the methodology proposed by Papadopoulos *et al.* (2011) and Varlas (2017) as shown in Figure 4. CHAOS is configured to a 30-h forecasting mode and 366 simulations have been conducted to cover the one-year period (1 simulation was utilized as a warm-up for the wave spectrum + 365 simulations for each day of the one-year period). The first simulation was initialized on the 30$^{th}$ of November 2013 at 00 UTC using ECMWF gridded analyses for the atmospheric parameters (as atmospheric initial conditions; AIC) and the SST field (as lower boundary condition over the sea). The "cold start" method was selected for the generation of the wave spectrum (as wave initial conditions; WIC). For the following days, each simulation was initialized at 00 UTC, based on the corresponding ECMWF analyses, while the ocean wave component was initialized in "hot start" mode based on the previous cycle wave spectrum estimation. This configuration implies that there is a 6-hour overlap between the simulations of two consecutive daily cycles. However, the first 6-hour period of each simulation is considered as the spin-up time of the models. As a result, the data produced during this period are considered of lower quality and, therefore, discarded as proposed by various studies (e.g. Lo *et al.,* 2008; Thompson *et al.,* 2016). Consequently, the model outputs that are actually considered in the final dataset of atmospheric and ocean wave parameters of the study are in the forecast window between the 6$^{th}$ and the 30$^{th}$ hour of each simulation.

## Data and Methods

A statistical software tool was developed in order to evaluate the results of the CHAOS simulations for the one-year period, focusing on the 2-way coupling effects on forecast skill. The performance of the 2-way coupling mode (2-way) is statistically evaluated not only over the sea, but also over land (since the air-sea interactions are

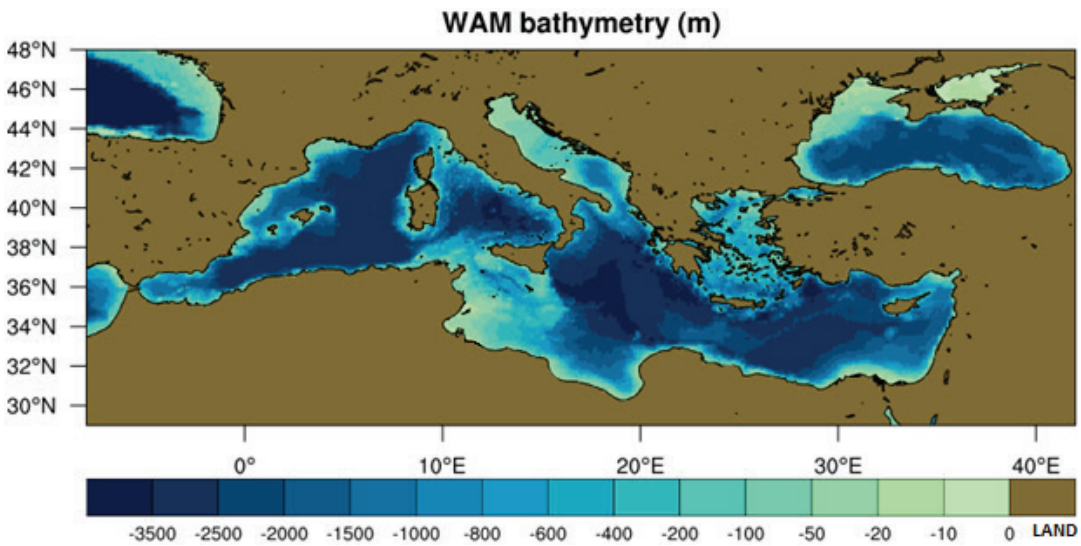


***Fig. 3:*** Illustration of the bathymetry (m) used by the WAM model (Varlas, 2017; Varlas *et al.,* 2018). The bathymetric map has been constructed from the Etopo1 database (Amante & Eakins, 2009; 1 min Gridded Global Relief Data).

**Table 1**. Configuration of atmospheric and ocean wave components of CHAOS.

| CHAOS | Atmospheric Component | Ocean Wave Component |
|---|---|---|
| Model | WRF-ARW, WRF-Chem V3.8 and WRF-Hydro V3.0 | WAM Cycle 4.5.4 |
| Coupler | OASIS3-MCT Version 3.0 | |
| Integration Domain | Mediterranean Sea, Europe, Black Sea | |
| Grid | Arakawa semi-staggered C-grid | Spherical latitude-longitude grid |
| Horizontal grid Increment | 10km x 10km | 0.1°x0.1° |
| Spectral resolution | – | 24 directional bins (15° directional resolution), 25 frequency bins (ranging from 0.042 to 0.411 Hz) |
| Vertical coordinate | Terrain-following hydrostatic pressure coordinate | – |
| Vertical levels | 38 | – |
| Time steps | 60 s | Propagation time step: 75 s<br>Source time step: 600 s |
| Initial & boundary Conditions | ECMWF, 0.5°x0.5°<br>17 isobaric levels<br>6h update of boundary conditions | Hot start |
| SST | ECMWF SST update every 6 hours | – |
| Exchange rate | 600 s | |
| Surface layer | Revised Monin-Obukhov | – |
| PBL | YSU | – |
| Microphysics | Thompson | – |
| Cumulus | Kain-Fritsch | – |
| Land surface | Unified NOAH | – |
| Radiation | RRTM and Dudhia schemes | – |
| Chemistry options | Disabled | – |
| Coupled to WRF-Hydro | Disabled | – |
| Topography | 30-arc-second USGS GMTED2010 | – |
| Vegetation | MODIS FPAR | – |
| Land-use | 21-class IGBP MODIS | – |
| Bathymetry | – | ETOPO1 |
| Water approximation | – | Shallow water approximation with depth refraction and wave breaking due to depth change near shore |

expected to change weather patterns and atmospheric conditions throughout the model domain) compared with its performance in the 1-way coupling mode (1-way), considered as control run. The meteorological variables used in the evaluation are near surface (at 10 meters) wind speed and significant wave height (SWH). The evaluation was performed against in situ observations and remote sensing data for a one-year period (1 December 2013 – 1 December 2014). The performance of CHAOS is assessed using 21 buoys in the Mediterranean Sea as reference, made available by CMEMS/Copernicus Med – In situ TAC (ftp://medinsitu.hcmr.gr/). The system was also evaluated against remote sensing data retrieved from the Jason-2 satellite distributed by Aviso (http://www.aviso.altimetry.fr/), as part of the SSALTO ground processing segment. Additionally, the sensitivity of the system was assessed over land, at almost 1000 surface meteorological stations across Europe, the Middle East and North Africa (ECMWF-GTS network; Fig. 5).

The evaluation methodology is based on a point-to-point hourly comparison between model-generated variables and observation data (Papadopoulos & Katsafados, 2009). The gridded outputs are interpolated at each buoy location, satellite retrieval and ground station using the nearest-neighbour interpolation scheme, and considering the nearest source point, sea or land-masked grid point. In this way, thousands of pairs of model outputs and observations were produced for both the 1-way and 2-way coupling modes. The evaluation procedure is based on the estimation of typical verification metrics such as the standard mean error (bias), and the root mean square error (RMSE) for wind speed and SWH. Moreover, the

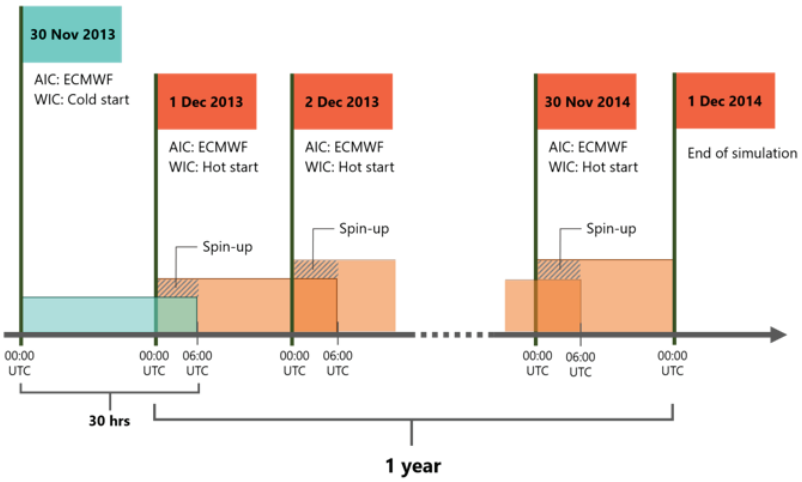


***Fig. 4:*** Long-term simulation timeline (Varlas, 2017). Each simulation is initialized at 00:00 UTC and lasts 30 hours starting on 30 November 2013 and ending on 1 December 2014. The crosshatched area represents the spin-up time (00:00-06:00 UTC) of each simulation. The atmospheric initial conditions (AIC) are based on ECMWF analyses while for wave initial conditions (WIC) "cold start" was applied for the 1st day and "hot start" for the rest of the days.

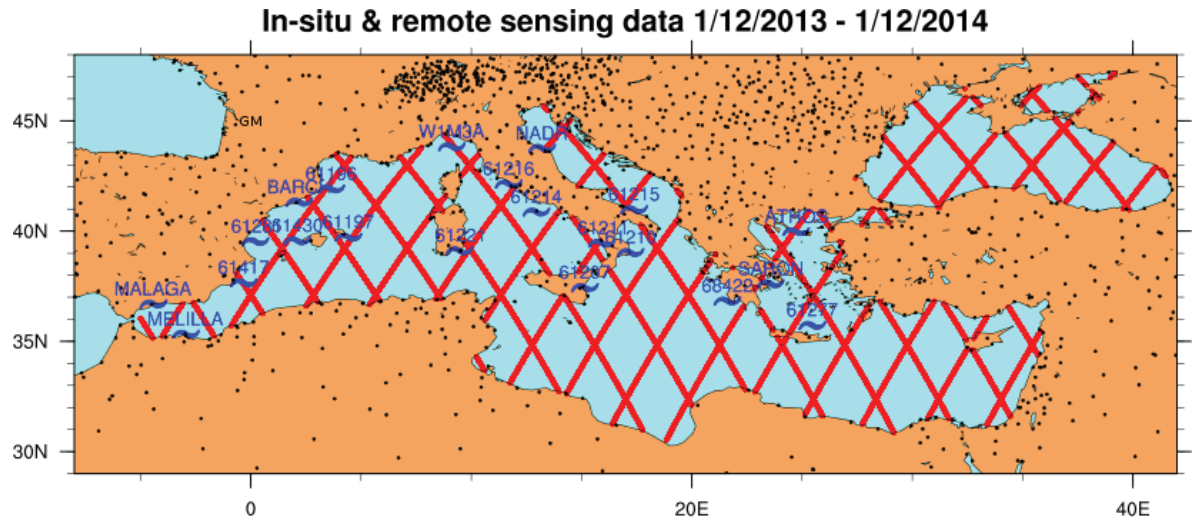


***Fig. 5:*** Spatial distribution of data applied for the evaluation of the system. Mediterranean buoys are shown in blue hyphens, Jason-2 satellite tracks with red lines and ECMWF-GTS stations with black dots.`

mean value (mean), standard deviation (STD) and Scatter Index (SI) were also calculated for both model and observed values. Supplementary scores include Pearson's correlation coefficient (CC) and the coefficient of determination ($R^2$). The formulas are described in detail in Wilks (2011). A Taylor diagram has also been used to visualize the overall performance of CHAOS. Taylor diagrams (Taylor, 2001) provide a graphical summary showing how close a pattern (or a set of patterns) matches the reference data.

## Results and Discussion

In this section, the performance of CHAOS over the one-year period, from 1 December 2013 to 1 December 2014, is evaluated using the methodology described above. At first, scatter plots are created for all the available data; these are presented in Figure 6 (a-c) for wind speed, the Mediterranean buoys, satellite data and inland ECMWF stations, while Figure 7 (a and b) presents SWH for the Mediterranean buoys and satellite data. For clarity purposes, the bias, RMSE, Pearson's CC, $R^2$ and SI scores are presented in Table 2. Moreover, the statistical scores for each buoy, wind speed and SWH are shown in Tables 3 and 4, respectively.

As far as wind speed evaluation based on the data obtained from ECMWF stations is concerned (Fig. 6c), it is evident that there are no differences between the scatter plots and derived statistics of the 1-way and 2-way simulations. This indicates that the main feedback from the ocean waves to the atmosphere is mostly isolated over the sea. Small differences at coastal stations (not presented here) are integrated over a large volume of inland data and thus such discrepancies are essentially lost. Therefore, we focus only on buoy and satellite data.

Overall, compared against buoy observations, a systematic overestimation of wind speed is evidenced for both simulations. The positive biases can be attributed to inaccuracies of the PBL and surface layer formulations in

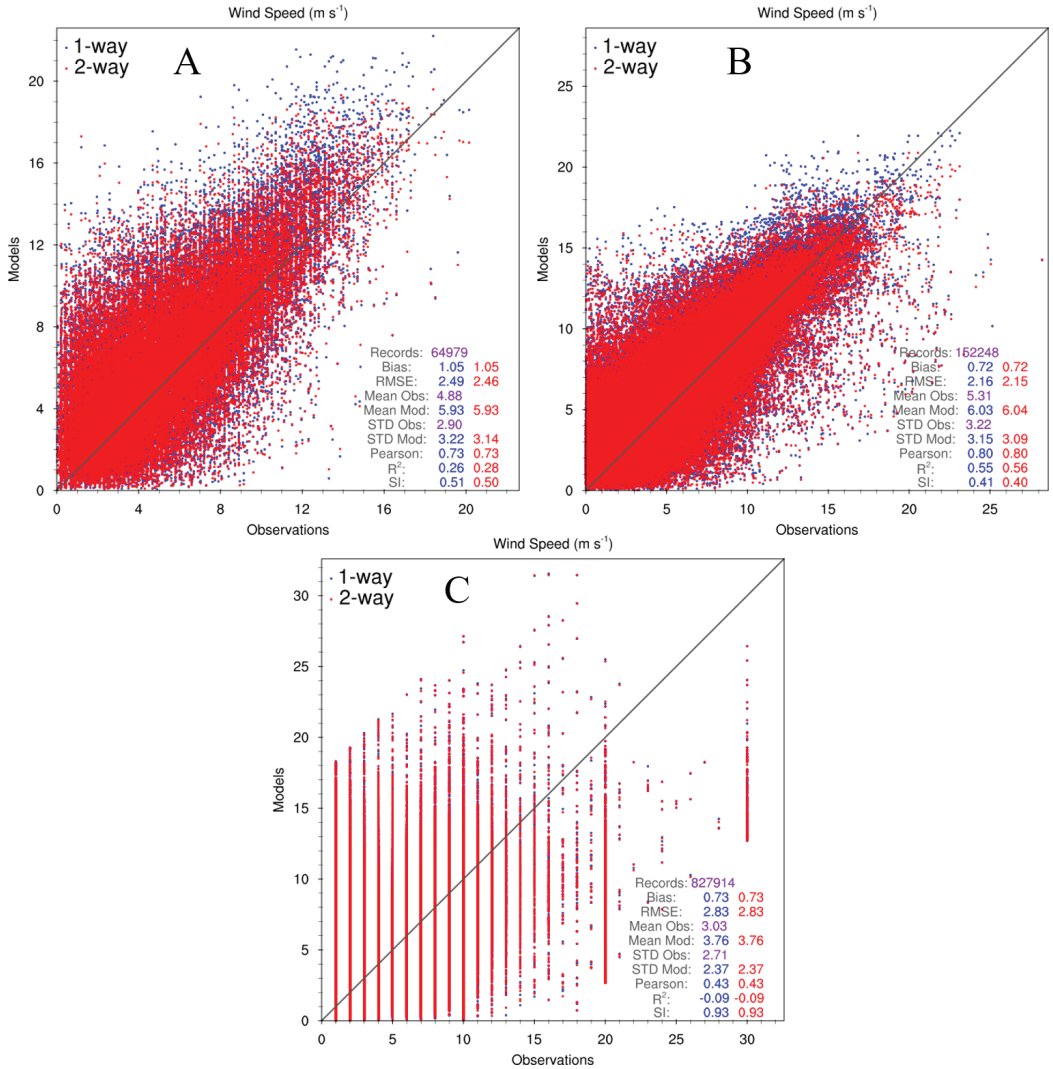


***Fig. 6:*** Scatter plots for wind speed (m $s^{-1}$) using data from (a) Mediterranean Buoys, (b) Satellite retrievals and (c) inland ECMWF stations. The Y-axis represents the model-estimated values and the X-axis the observations. The 1-way and 2-way simulation results are depicted in blue and red, respectively.

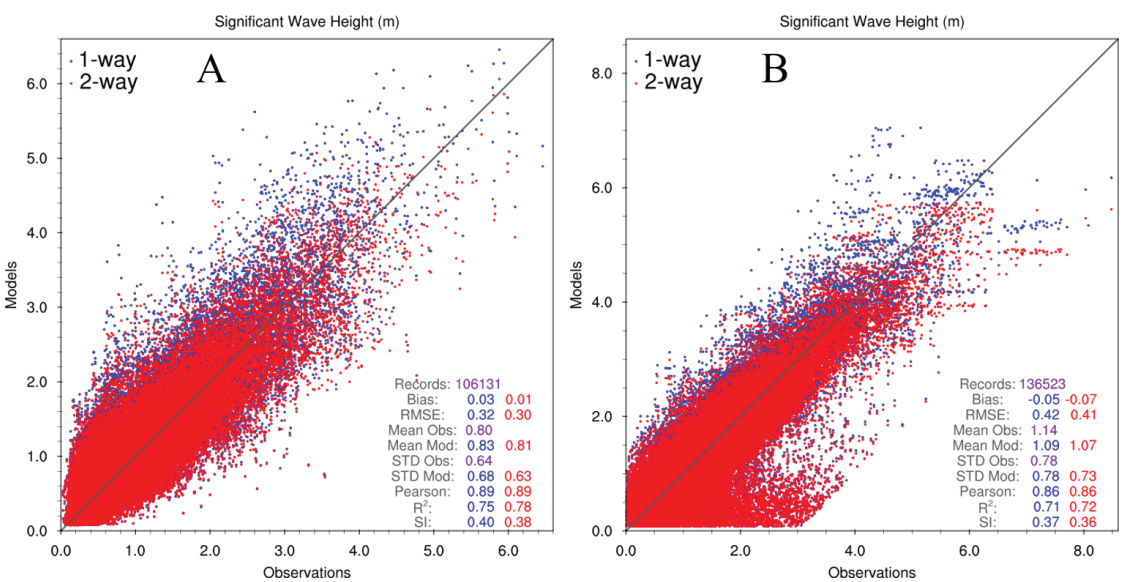


***Fig. 7:*** Scatter plots for SWH (m) using data from (a) Mediterranean Buoys and (b) Satellite retrievals. The Y-axis represents the model-estimated values and the X-axis the observations. The 1-way and 2-way simulation results are depicted in blue and red, respectively.

**Table 2**. Statistical scores for wind speed (Wind Buoys and Wind Sat) and SWH (Wave buoys and Wave Sat). The percentage of the change in the statistical scores between 2-way and 1-way simulations is also presented.

| | Wind Buoys | | | Wind SAT | | | Wave Buoys | | | Wave SAT | | |
|---|---|---|---|---|---|---|---|---|---|---|---|---|
| | 1-way | 2-way | % | 1-way | 2-way | % | 1-way | 2-way | % | 1-way | 2-way | % |
| Bias | 1.05 | 1.05 | - | 0.72 | 0.72 | - | 0.03 | 0.01 | - | -0.05 | -0.07 | - |
| RMSE | 2.49 | 2.46 | -1.2 | 2.16 | 2.15 | -0.5 | 0.32 | 0.30 | -6.3 | 0.42 | 0.41 | -2.4 |
| Pearson | 0.73 | 0.73 | 0 | 0.80 | 0.80 | 0 | 0.89 | 0.89 | 0 | 0.86 | 0.86 | 0 |
| $R^2$ | 0.26 | 0.28 | 7.7 | 0.55 | 0.56 | 1.8 | 0.75 | 0.78 | 4 | 0.71 | 0.72 | 1.4 |
| SI | 0.51 | 0.50 | -2 | 0.41 | 0.40 | -2.4 | 0.40 | 0.38 | -5 | 0.37 | 0.36 | -2.7 |

**Table 3**. Statistical scores for wind speed for each individual buoy in the Mediterranean Sea.

| Buoy | Records | Wind speed (m $s^{-1}$) | | | | | | | | | |
|---|---|---|---|---|---|---|---|---|---|---|---|
| | | Bias | | RMSE | | Pearson | | $R^2$ | | SI | |
| | | 1-way | 2-way | 1-way | 2-way | 1-way | 2-way | 1-way | 2-way | 1-way | 2-way |
| 61214 | 28 | -0.42 | -0.41 | 2.82 | 2.83 | 0.02 | 0.05 | -1.11 | -1.12 | 0.76 | 0.77 |
| SARON | 2720 | 1.39 | 1.40 | 2.80 | 2.79 | 0.63 | 0.63 | -0.03 | -0.03 | 0.63 | 0.63 |
| W1M3A | 1461 | 0.68 | 0.69 | 2.73 | 2.71 | 0.64 | 0.64 | 0.13 | 0.14 | 0.59 | 0.59 |
| 61196 | 4521 | 1.32 | 1.21 | 2.79 | 2.65 | 0.83 | 0.82 | 0.43 | 0.49 | 0.44 | 0.42 |
| 61197 | 8382 | 1.16 | 1.17 | 2.27 | 2.26 | 0.79 | 0.79 | 0.38 | 0.39 | 0.45 | 0.45 |
| 61281 | 8054 | 0.93 | 0.93 | 2.36 | 2.34 | 0.72 | 0.72 | 0.28 | 0.29 | 0.52 | 0.51 |
| 61417 | 8609 | 1.33 | 1.33 | 2.33 | 2.30 | 0.80 | 0.79 | 0.29 | 0.30 | 0.49 | 0.48 |
| 61430 | 7460 | 0.86 | 0.87 | 2.44 | 2.42 | 0.71 | 0.71 | 0.26 | 0.28 | 0.51 | 0.51 |
| BARCH | - | - | - | - | - | - | - | - | - | - | - |
| MALAGA | - | - | - | - | - | - | - | - | - | - | - |
| MELILLA | - | - | - | - | - | - | - | - | - | - | - |
| 61277 | 958 | 1.21 | 1.19 | 2.76 | 2.71 | 0.69 | 0.69 | 0.22 | 0.25 | 0.51 | 0.50 |
| 68422 | 2556 | 1.69 | 1.69 | 2.91 | 2.87 | 0.69 | 0.69 | -0.21 | -0.18 | 0.64 | 0.63 |
| ATHOS | 1897 | 1.68 | 1.68 | 2.98 | 2.95 | 0.66 | 0.66 | -0.27 | -0.25 | 0.72 | 0.72 |
| 61221 | 3512 | 1.03 | 1.02 | 2.76 | 2.74 | 0.65 | 0.64 | 0.09 | 0.11 | 0.50 | 0.49 |
| 61207 | 33 | -0.57 | -0.66 | 2.45 | 2.40 | 0.70 | 0.71 | 0.36 | 0.38 | 0.43 | 0.42 |
| 61211 | - | - | - | - | - | - | - | - | - | - | - |
| 61216 | 4529 | 0.59 | 0.60 | 2.14 | 2.14 | 0.72 | 0.71 | 0.31 | 0.30 | 0.46 | 0.46 |
| 61210 | - | - | - | - | - | - | - | - | - | - | - |
| 61215 | 5377 | 0.52 | 0.54 | 2.10 | 2.08 | 0.76 | 0.75 | 0.45 | 0.46 | 0.41 | 0.41 |
| NADR | 4881 | 1.00 | 1.01 | 2.80 | 2.79 | 0.50 | 0.50 | -0.23 | -0.22 | 0.65 | 0.65 |

WRF (Katsafados *et al.,* 2011; Shimada & Ohsawa, 2011; Jiménez *et al.,* 2012). However, as presented in Figure 6a and Table 2, the results of the 2-way simulation reveal a reduction of the RMSE (1.2%), improving the $R^2$ (7.7%) and SI (2%). The overall improvement in wind speed has a positive effect on SWH (Fig. 7a; Table 2). Thus, the 2-way run reduces the bias and RMSE (6.3%) while improving the $R^2$ (4%) and SI (5%). Additionally, Pearson's CC of the 2-way simulation is almost identical with the 1-way run. The results are characterized by a high confidence level (>95%).

Systematic overestimation of wind speed is attenuated when evaluation is performed against satellite retrievals. This may be attributed to the fact that satellite retrievals refer to offshore areas and fit model gridded values better than buoy measurements since they represent area-averaged values. On the other hand, Mediterranean Sea buoys are usually at nearshore locations where simulation errors are exaggerated due to inadequate representation of complex coastlines and inaccurate calculation of shallow water wave reflection. It is interesting to note that for the Balearic Sea buoy 61196 the 1-year RMSE reductions of the 2-way coupling mode for wind speed and SWH reach 5% and 9.5%, respectively (Tables 3 and 4; Figs. 5 and 9a). An explanation for this boost in performance may be the significant sea state effect of strong Mistral winds over this area, which limits overestimation resulting from the 1-way coupling mode.

Compared against satellite retrievals, Figure 6b indicates that overestimation is more prominent for lower wind speeds and that the 2-way coupling mode offers an overall improvement in wind speed ranging from 0.5% reduction of the RMSE to 2.4% reduction of the SI (Table 2). Moreover, 2-way simulation produced a 2.4% reduction of the RMSE and a 2.7% reduction of the SI in the estimation of SWH (Fig. 7b; Table 2). However, the 2-way coupling mode produced slightly stronger underestimation compared to the 1-way mode. This could be attributed to the fact that remotely sensed SWH is characterized by systematic overestimation compared to buoy

**Table 4**. Statistical scores for SWH for each individual buoy in the Mediterranean Sea.

| Buoy | Records | SWH (m) | | | | | | | | | |
|---|---|---|---|---|---|---|---|---|---|---|---|
| | | Bias | | RMSE | | Pearson | | $R^2$ | | SI | |
| | | 1-way | 2-way | 1-way | 2-way | 1-way | 2-way | 1-way | 2-way | 1-way | 2-way |
| 61214 | 5104 | 0.03 | 0.02 | 0.31 | 0.29 | 0.90 | 0.91 | 0.79 | 0.82 | 0.37 | 0.35 |
| SARON | 2675 | 0.08 | 0.08 | 0.28 | 0.26 | 0.81 | 0.81 | -0.04 | 0.07 | 0.61 | 0.57 |
| W1M3A | - | - | - | - | - | - | - | - | - | - | - |
| 61196 | 8717 | 0.08 | 0.03 | 0.42 | 0.38 | 0.90 | 0.90 | 0.75 | 0.80 | 0.36 | 0.32 |
| 61197 | 8283 | -0.02 | -0.05 | 0.32 | 0.32 | 0.93 | 0.93 | 0.86 | 0.86 | 0.26 | 0.25 |
| 61281 | 5850 | 0.04 | 0.02 | 0.30 | 0.27 | 0.80 | 0.81 | 0.48 | 0.56 | 0.38 | 0.35 |
| 61417 | 8709 | -0.06 | -0.08 | 0.31 | 0.31 | 0.88 | 0.88 | 0.75 | 0.75 | 0.30 | 0.30 |
| 61430 | 7627 | 0.04 | 0.01 | 0.32 | 0.30 | 0.90 | 0.90 | 0.78 | 0.80 | 0.34 | 0.32 |
| BARCH | 8594 | -0.09 | -0.10 | 0.26 | 0.26 | 0.85 | 0.85 | 0.66 | 0.66 | 0.36 | 0.35 |
| MALAGA | 6750 | 0.10 | 0.10 | 0.34 | 0.32 | 0.82 | 0.82 | -0.11 | 0.04 | 0.77 | 0.71 |
| MELILLA | 8397 | 0.24 | 0.22 | 0.41 | 0.38 | 0.81 | 0.82 | 0.25 | 0.34 | 0.81 | 0.76 |
| 61277 | 1952 | 0.07 | 0.06 | 0.32 | 0.30 | 0.89 | 0.89 | 0.75 | 0.77 | 0.30 | 0.29 |
| 68422 | 1887 | 0.01 | 0.00 | 0.32 | 0.30 | 0.89 | 0.89 | 0.76 | 0.79 | 0.33 | 0.31 |
| ATHOS | 1407 | 0.03 | 0.01 | 0.29 | 0.27 | 0.92 | 0.91 | 0.81 | 0.82 | 0.35 | 0.33 |
| 61221 | 5398 | 0.11 | 0.11 | 0.29 | 0.28 | 0.82 | 0.82 | 0.52 | 0.55 | 0.47 | 0.45 |
| 61207 | 4304 | -0.23 | -0.23 | 0.34 | 0.35 | 0.87 | 0.87 | 0.52 | 0.50 | 0.59 | 0.61 |
| 61211 | 5333 | 0.02 | 0.01 | 0.26 | 0.25 | 0.91 | 0.91 | 0.81 | 0.82 | 0.40 | 0.38 |
| 61216 | 4529 | 0.03 | 0.02 | 0.22 | 0.21 | 0.90 | 0.90 | 0.79 | 0.81 | 0.36 | 0.35 |
| 61210 | 5238 | 0.04 | 0.03 | 0.26 | 0.25 | 0.92 | 0.92 | 0.82 | 0.84 | 0.37 | 0.35 |
| 61215 | 5377 | -0.01 | -0.01 | 0.26 | 0.25 | 0.89 | 0.89 | 0.71 | 0.74 | 0.40 | 0.37 |
| NADR | - | - | - | - | - | - | - | - | - | - | - |

observations (Abdalla *et al*., 2010). For that reason, both simulations present lower bias against remotely sensed data than against buoy measurements and thus they result to underestimation more pronounced for the 2-way mode. Moreover, Figure 7b illustrates a negative bias bulge with satellite retrievals at 2-3 m SWH, which is attributed to the inadequacy of satellite retrievals and the wave model to estimate the nearshore sea state accurately.

Figure 8 presents a Taylor diagram (Taylor, 2001) summarizing the evaluation results. In Taylor diagrams, the similarity between two patterns is quantified in terms of their Pearson's CC, centred root mean square (RMS) difference (or error) and the amplitude of their variations (represented by their normalized standard deviations). The standard deviation (STD) of the simulated pattern is proportional to the radial distance from the reference circle intersecting the X-axis at "REF". It is important to note that the STD of the observation data was used for the normalization of the simulated STD values. Additionally, the centred (RMS) difference between the simulated and observed patterns is proportional to the distance from "REF", while Pearson's CC is identical (equal to 1) on the X-axis.

Hence, the models producing evaluation scores near "REF" are more skilful. In this study, Pearson's CC, the normalized STD and the normalized centred RMS difference are illustrated in blue and red on the Taylor diagram, for 1-way and 2-way simulations, respectively. The Taylor diagram confirms the improved overall performance of the 2-way coupling mode. The positions of dots 1, 2, 3 and 4 indicate that the 2-way mode outperforms the 1-way mode, reducing the centred RMS difference and

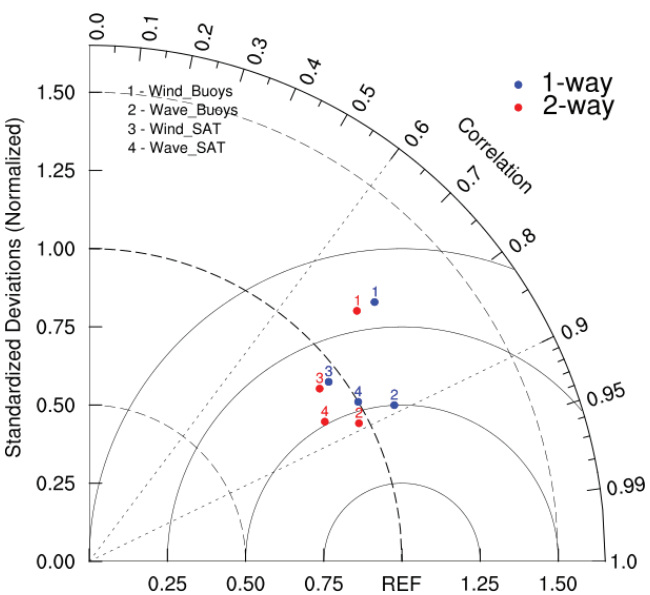


***Fig. 8:*** Taylor diagram for wind speed (m $s^{-1}$) and SWH (m). 1-2 refer to the comparison with buoy observations and 3-4 to the comparison with satellite retrievals. The 1-way and 2-way simulation results are depicted in blue and red, respectively.

coming closer to "REF".

Integration of statistical scores over a long period usually hides the variations and peaks of the forecasting skill and model capabilities. Better statistical scores are observed at some buoys during periods characterized by extreme weather events, e.g. in the case of the Balearic Sea buoy 61196 (Tables 3 and 4; Figs. 5 and 9a), the 2-way coupling mode offers larger improvements under high wind and sea state conditions compared to overall performance (Fig. 9c). Specifically, for a 4-day period, from 21 to 25 October 2014, which was characterized by gale-force north-western Mistral winds and high waves over the Balearic Sea, the 2-way coupling mode offers wind speed and SWH improvements (RMSE reduction) of up to 12% and 34%, respectively (Fig. 9b).

On the other hand, for wind speed and SWH, 1-year RMSE reductions of up to 5% and 9.5% are noted, respectively (Fig. 9c). Thus, the 1-year improvements are smaller than the improvements under high wind and sea state conditions. This difference indicates that the 2-way coupling reduces the forecast error to a large degree mainly in cases of high wind and sea state conditions, while 1-way coupling is characterized by systematic overestimation. This is attributed to the dependence of 2-way coupling on the application of Charnock parameterization, which is more crucial in a range from medium to high wind and wave intensities (e.g. Desjardins *et al.,* 2000; Katsafados *et al.,* 2016; Wahle *et al.,* 2017; Varlas *et al.,* 2018).

In order to assess the spatial distribution of the percentage of the change in the RMSE between the 2-way and 1-way coupling modes, the data is analyzed on a grid,

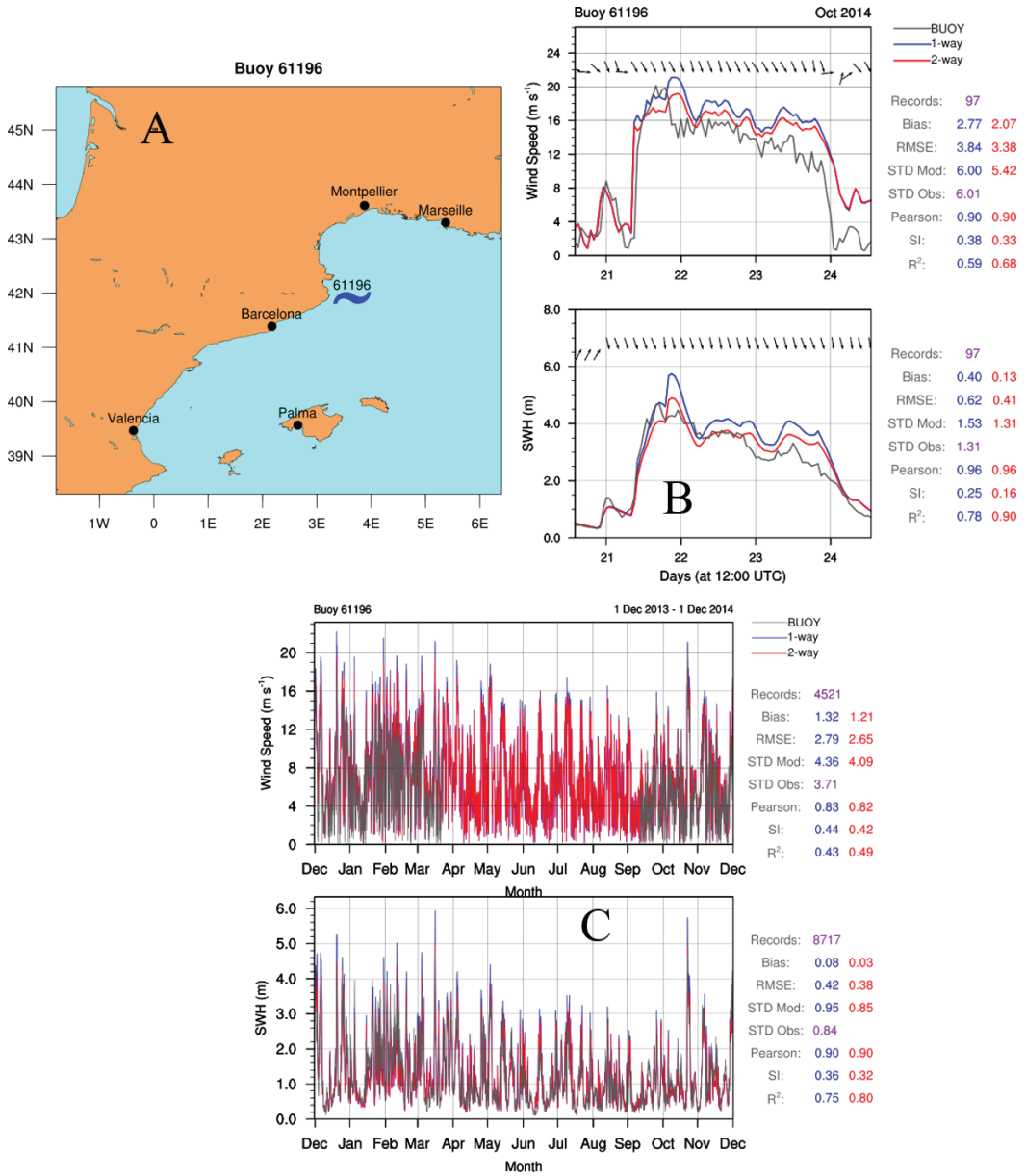


***Fig. 9:*** (a) Location of Mediterranean buoy 61196. Time series of wind speed (m $s^{-1}$) and SWH (m) based on the observations of Mediterranean buoy 61196 (gray), 1-way (blue) and 2-way (red) simulations. The results of statistical evaluation, based on the calculation of statistical indices, are illustrated on the right. Time period (b) from 21 October at 00:00 UTC to 25 October at 00:00 UTC, 2014. The black arrows represent wind and SWH directions, measured by the buoy. (c) Time period from 1 December at 00:00 UTC, 2013 to 1 December at 00:00 UTC, 2014.

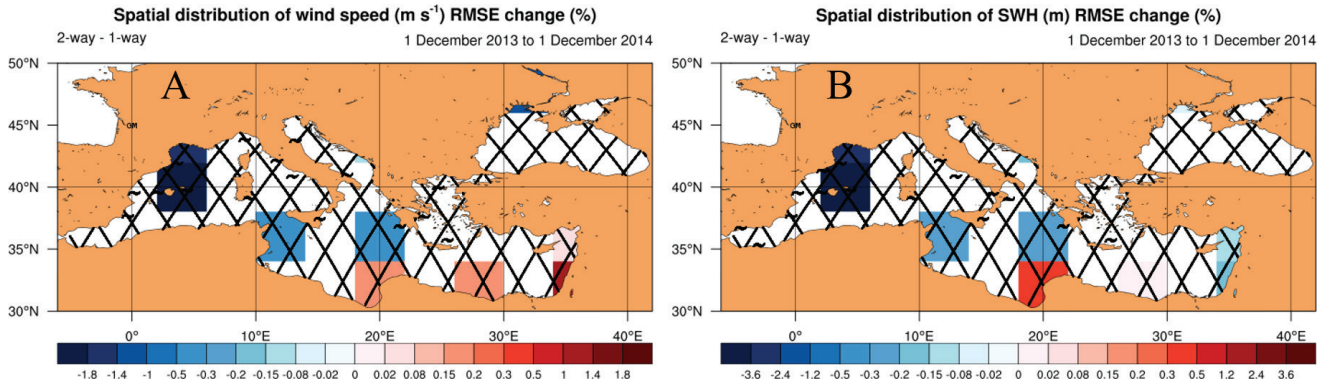


***Fig. 10:*** RMSE change (%) for (a) wind speed and (b) SWH, compared against buoy observations and Jason-2 satellite retrievals. Buoys and Jason-2 satellite tracks are superimposed on the maps with black hyphens and black lines, respectively.

in horizontal resolution of 4°×4° (Figs. 10 a and b) using the formula below (Eq. 3):

$$\text{RMSE change (\%)} = 100 \times \frac{\text{RMSE(2way)} - \text{RMSE(1way)}}{\text{RMSE(1way)}}$$

The use of a horizontal grid to spatially analyze statistical indices is also applied by Varlas *et al.* (2019b). In Figure 10 (a and b), the buoys and Jason-2 satellite tracks are superimposed on the maps with black hyphens and black lines, respectively. The highest reduction of RMSE is observed in the Balearic Sea and the Gulf of Lion, reaching 1.8% for wind speed (Fig. 10a) and 3.7% for SWH (Fig. 10b). The improvements are greater when the evaluation is performed only against buoy observations. The RMSE reduction is lower when satellite data is aggregated in each cell. In the other evaluation grid cells of the Mediterranean and Black Seas there are small variations of the RMSE change. The majority of grid cells show either similar RMSE for the two simulations or dominance of the 2-way coupling mode, excluding a few nearshore areas in the south-eastern Mediterranean where the opposite pattern, for wind speed mainly, is presented. The results of spatial analysis of the RMSE change indicate that 2-way coupling yields statistical improvements mainly over areas characterized by intense atmospheric flow and fresh wave growth. The northern Balearic Sea and the Gulf of Lion are characterized by the more intense winds in the Mediterranean Sea (Soukissian *et al.,* 2017). Moreover, the Mistral winds originating from the land rapidly strike the sea and generate high-frequency wind-waves across a long-fetch area. Under these conditions, the 2-way coupling mode unveils its capability to offer more realistic wind and wave data through the encapsulation of sea state information in the atmospheric surface layer processes.

## Conclusions

In this study, we provide a statistical assessment of the one-year forecast skill of an advanced two-way coupled atmosphere-ocean wave modelling system, namely CHAOS. To this end, the system was set up to perform continuous 30-h simulations during a one-year period (1 December 2013 - 1 December 2014) in 1-way (no ocean wave information was considered in atmospheric surface layer processes) and 2-way coupling mode. Both sets of simulations were evaluated using Mediterranean buoy observations, satellite retrievals and inland ECMWF station observations. The latter were found to provide no insight on the effects of waves on wind speed, as they were mostly far from coastal areas, where the effects of waves have an influence. Thus, only buoy and remote sensing data were considered.

The statistical scores of wind speed and significant wave height over the sea produced by the 1-way (control) and 2-way coupling modes compared against buoy observations and satellite retrievals show that the 2-way coupling mode produces significant improvements in cases characterized by intense wind and sea state conditions. This finding is in agreement with Katsafados *et al.* (2016) and Varlas *et al.* (2018). Compared against buoy observations, the one-year RMSE reduction reaches 1.2% and 6.3% for wind speed and significant wave height, respectively, while compared against Jason-2 satellite retrievals they reach 0.5% and 2.4%, respectively. However, the evaluation during extreme weather sub-periods of the 1 December 2013 - 1 December 2014 period reveals higher statistical improvements. This is attributed to the fact that the integration of statistical scores over a long period usually hides the variations and peaks of the forecast skill. Low and moderate wind and wave conditions are dominant in a one-year operational approach reducing the improvements of the forecast skill attributed to the higher intensities, characterized by more an intense 2-way coupling effect.

Concerning buoy 61196 located in the Balearic Sea, it is interesting to note that the 1-year improvements for wind speed and SWH reach 5% and 9.5%, respectively; 2-way coupling improvements are evidenced especially over areas characterized by intense atmospheric flows such as the Mistral winds in the Gulf of Lion. This is due to the fact that wave spectrum intensity is dependent on wind-generated waves and, consequently, near surface wind speed and fetch (Janssen, 2004). During wind-wave generation, the surface layer of 2-way coupled simulations incorporates rougher sea surface information compared to the 1-way coupling mode using the constant

Charnock parameter. This causes a reduction of wind speed and intense attenuation of high-frequency waves and, subsequently, of significant wave height. This reduction mechanism is more prominent over windy long-fetch areas than over short-fetch areas near the shore that is characterized by low to moderate wind-waves. Moreover, wave growth depends on the square of near surface wind speed and, thus, a small decrease of wind speed can cause a more intense decrease of significant wave height. This could explain the higher statistical improvements produced by the 2-way coupling mode in the estimation of SWH rather than wind speed.

This study is a successful first step towards the long-term statistical assessment of the CHAOS two-way coupled atmosphere-ocean wave modelling system. The authors' future plans include a long-term statistical assessment of 2-way coupling effects on additional parameters such as air-sea heat fluxes, humidity, and precipitation at basin scale, as well as on the implementation of extreme wave estimation (e.g. Barbariol *et al.,* 2019), especially in the context of a variable climate. Moreover, the findings of this work encourage the authors to further investigate air-sea interaction incorporating an ocean circulation model in CHAOS.

## Acknowledgements

The European Centre for Medium-Range Weather Forecasts (ECMWF) is gratefully acknowledged for the kind provision of the gridded analyses data and land surface observations. The CMEMS/Copernicus Med – in situ TAC and AVISO are also acknowledged for the provision of buoy and satellite data, respectively. The Greek Research and Technology Network (GRNET) is acknowledged for the access to the high-performance computer (HPC) ARIS (https://hpc.grnet.gr/), where the simulations of this study were performed. Finally, part of this study was conducted using E.U. Copernicus Marine Service Information.

## References

Abdalla, S., Janssen, P.A., Bidlot, J. R., 2010. Jason-2 OGDR wind and wave products: Monitoring, validation and assimilation. *Marine Geodesy*, 33 (S1), 239-255.

Amante, C., Eakins, B.W., 2009. *ETOPO1 1 arc-minute global relief model: procedures, data sources and analysis*. Colorado: US Department of Commerce, National Oceanic and Atmospheric Administration, National Environmental Satellite, Data, and Information Service, National Geophysical Data Center, Marine Geology and Geophysics Division, 19 pp.

Andreas, E.L., 2011. Fallacies of the enthalpy transfer coefficient over the ocean in high winds. *Journal of the Atmospheric Sciences*, 68 (7), 1435-1445.

Bao, J.W., Fairall, C.W., Michelson, S.A., Bianco, L., 2011. Parameterizations of sea-spray impact on the air-sea momentum and heat fluxes. *Monthly Weather Review*, 139 (12), 3781-3797.

Barbariol, F., Benetazzo, A., Bertotti, L., Cavaleri, L., Durrant, T. *et al.,* 2019. Large waves and drifting buoys in the Southern Ocean. *Ocean Engineering*, 172, 817-828.

Battjes, J.A., Janssen, J.P.F.M., 1978. Energy loss and set-up due to breaking of random waves. p. 569-587. In *Proceedings of the 16th International Conference on Coastal Engineering*. American Society of Civil Engineers, New York.

Bell, M.M., Montgomery, M.T., Emanuel, K.A., 2012. Air–sea enthalpy and momentum exchange at major hurricane wind speeds observed during CBLAST. *Journal of the Atmospheric Sciences*, 69 (11), 3197-3222.

Benetazzo, A., Bergamasco, A., Bonaldo, D., Falcieri, F. M., Sclavo, M. *et al.,* 2014. Response of the Adriatic Sea to an intense cold air outbreak: dense water dynamics and wave-induced transport. *Progress in Oceanography*, 128, 115-138.

Black, P.G., D'Asaro, E.A., Sanford, T.B., Drennan, W.M., Zhang, J.A. *et al.,* 2007. Air-sea exchange in hurricanes: synthesis of observations from the coupled boundary layer air-sea transfer experiment. *Bulletin of the American Meteorological Society*, 88 (3), 357-374.

Bonaldo, D., Antonioli, F., Archetti, R., Bezzi, A., Correggiari, A. *et al.,* 2019. Integrating multidisciplinary instruments for assessing coastal vulnerability to erosion and sea level rise: Lessons and challenges from the Adriatic Sea, Italy. *Journal of Coastal Conservation*, 23 (1), 19-37.

Breivik, Ø., Mogensen, K., Bidlot, J.R., Balmaseda, M.A., Janssen, P.A., 2015. Surface wave effects in the NEMO ocean model: Forced and coupled experiments. *Journal of Geophysical Research: Oceans*, 120 (4), 2973-2992.

Bruneau, N., Toumi, R., 2016. A fully-coupled atmosphere-ocean-wave model of the Caspian Sea. *Ocean Modelling*, 107, 97-111.

Carniel, S., Benetazzo, A., Bonaldo, D., Falcieri, F.M., Miglietta, M.M. *et al.,* 2016. Scratching beneath the surface while coupling atmosphere, ocean and waves: Analysis of a dense water formation event. *Ocean Modelling*, 101, 101-112.

Chen, S.S., Zhao, W., Donelan, M.A., Tolman, H.L., 2013. Directional wind-wave coupling in fully coupled atmosphere-wave-ocean models: Results from CBLAST-Hurricane. *Journal of the Atmospheric Sciences*, 70 (10), 3198-3215.

Christakos, K., Cheliotis, I., Varlas, G., Steeneveld, G.J., 2016. Offshore wind energy analysis of cyclone Xaver over North Europe. *Energy Procedia*, 94, 37-44.

Christakos, K., Varlas, G., Reuder, J., Katsafados, P., Papadopoulos, A., 2014. Analysis of a low-level coastal jet off the western coast of Norway. *Energy Procedia*, 53, 162-172.

Danielson, J.J., Gesch, D.B., 2011. *Global multi-resolution terrain elevation data 2010 (GMTED2010)*. US Geological Survey, No 2011-1073, 34 pp. (Online available at: https://pubs.usgs.gov/of/2011/1073/pdf/of2011-1073.pdf, accessed 19.11.2018)

Desjardins, S., Mailhot, J., Lalbeharry, R., 2000. Examination of the impact of a coupled atmospheric and ocean wave system. Part I: Atmospheric aspects. *Journal of Physical Oceanography*, 30 (2), 385-401.

Donelan, M.A., Haus, B.K., Reul, N., Plant, W.J., Stiassnie, M. *et al.,* 2004. On the limiting aerodynamic roughness of the ocean in very strong winds. *Geophysical Research Letters*, 31 (18).

Doyle, J.D., 1995. Coupled ocean wave/atmosphere mesoscale model simulations of cyclogenesis. *Tellus A*, 47 (5), 766-778.

Drennan, W.M., Zhang, J.A., French, J.R., McCormick, C., Black, P.G., 2007. Turbulent fluxes in the hurricane boundary layer. Part II: Latent heat flux. *Journal of the Atmospheric Sciences*, 64 (4), 1103-1115.

Dudhia, J., 1989. Numerical study of convection observed during the winter monsoon experiment using a mesoscale two-dimensional model. *Journal of the Atmospheric Sciences*, 46 (20), 3077-3107.

Fairall, C.W., Bradley, E.F., Hare, J.E., Grachev, A.A., Edson, J.B., 2003. Bulk parameterization of air-sea fluxes: Updates and verification for the COARE algorithm. *Journal of Climate*, 16 (4), 571-591.

French, J.R., Drennan, W.M., Zhang, J.A., Black, P.G., 2007. Turbulent fluxes in the hurricane boundary layer. Part I: Momentum flux. *Journal of the Atmospheric Sciences*, 64 (4), 1089-1102.

Friedl, M.A., Sulla-Menashe, D., Tan, B., Schneider, A., Ramankutty, N. *et al.,* 2010. MODIS Collection 5 global land cover: Algorithm refinements and characterization of new datasets. *Remote sensing of Environment*, 114 (1), 168-182.

Gochis, D.J., Yu, W., Yates, D.N., 2015. *The WRF-Hydro model technical description and user's guide, version 3.0*. NCAR Technical Document, Boulder, Colorado, USA, 123 pp. (Online available at: https://ral.ucar.edu/sites/default/files/public/images/project/WRF_Hydro_User_Guide_v3.0.pdf, accessed 19.11.2018)

Grell, G.A., Peckham, S.E., Schmitz, R., McKeen, S.A., Frost, G. *et al.,* 2005. Fully coupled "online" chemistry within the WRF model. *Atmospheric Environment*, 39 (37), 6957-6975.

Hodur, R.M., 1997. The Naval Research Laboratory's coupled ocean/atmosphere mesoscale prediction system (COAMPS). *Monthly Weather Review*, 125 (7), 1414-1430.

Hong, S.-Y., Noh, Y., Dudhia, J., 2006. A new vertical diffusion package with an explicit treatment of entrainment processes. *Monthly Weather Review*, 134, 2318-2341.

Janssen, P., 2004. *The interaction of ocean waves and wind*. Cambridge University Press, London, UK, 310 pp.

Janssen, P.A., 1989. Wave-induced stress and the drag of air flow over sea waves. *Journal of Physical Oceanography*, 19 (6), 745-754.

Janssen, P.A.E.M., 1991. The Quasi-linear theory of wind wave generation applied to wave forecasting. *Journal of Physical Oceanography*, 21, 1631-1642.

Janssen, P.A.E.M., Doyle, J.D., Bidlot, J., Hansen, B., Isaksen, L. *et al.,* 2002. Impact and feedback of ocean waves on the atmosphere. *Advances in Fluid Mechanics*, 33, 155-198.

Jenkins, A.D., Paskyabi, M.B., Fer, I., Gupta, A., Adakudlu, M., 2012. Modelling the effect of ocean waves on the atmospheric and ocean boundary layers. *Energy Procedia*, 24, 166-175.

Jiménez, P.A., Dudhia, J., González-Rouco, J.F., Navarro, J., Montávez, J.P. *et al.,* 2012. A revised scheme for the WRF surface layer formulation. *Monthly Weather Review*, 140 (3), 898-918.

Kain, J. S., 2004. The Kain-Fritsch convective parameterization: an update. *Journal of Applied Meteorology*, 43 (1), 170-181.

Katsafados, P., Papadopoulos, A., Korres, G., Varlas, G., 2016. A fully coupled atmosphere-ocean wave modeling system for the Mediterranean Sea: interactions and sensitivity to the re-solved scales and mechanisms. *Geoscientific Model Development*, 9 (1), 161-173.

Katsafados, P., Papadopoulos, A., Mavromatidis, E., Gikas, N., 2011. Quantitative verification statistics of WRF predictions over the Mediterranean region. In: *12th Annual WRF Users' Event*, *20-24 June 2011*. Boulder, Colorado, USA, 6 pp.

Katsafados, P., Varlas, G., Papadopoulos, A., Korres, G., 2017. Implementation of a Hybrid Surface Layer Parameterization Scheme for the Coupled Atmosphere-Ocean Wave System WEW. p. 159-165. In: *Perspectives on Atmospheric Sciences*. Karacostas, T., Bais, A., Nastos, P. (Eds), Springer, Cham.

Katsafados, P., Varlas, G., Papadopoulos, A., Spyrou, C., Korres, G., 2018. Assessing the implicit rain impact on sea state during hurricane Sandy (2012). *Geophysical Research Letters,* 45, 12015-12022.

Komen, G. J., Cavaleri, L., Donelan, M., Hasselmann, K., Hasselmann, S. *et al.,* 1994. *Dynamics and modeling of ocean waves.* Cambridge university press, Cambridge, UK, 532 pp.

Korres, G., Papadopoulos, A., Katsafados, P., Ballas, D., Perivoliotis, L. *et al.,* 2011. A 2-year intercomparison of the WAM-Cycle4 and the WAVEWATCH-III wave models implemented within the Mediterranean Sea. *Mediterranean Marine Science*, 12 (1), 129-152.

Ličer, M., Smerkol, P., Fettich, A., Ravdas, M., Papapostolou, A. *et al.,* 2016. Modeling the ocean and atmosphere during an extreme bora event in northern Adriatic using one-way and two-way atmosphere-ocean coupling. *Ocean Science*, 12 (1), 71-86.

Lo, J.C.F., Yang, Z.L., Pielke, R.A., 2008. Assessment of three dynamical climate downscaling methods using the Weather Research and Forecasting (WRF) model. *Journal of Geophysical Research: Atmospheres*, 113 (D9).

Mlawer, E. J., Taubman, S. J., Brown, P. D., Iacono, M. J., Clough, S. A., 1997. Radiative transfer for inhomogeneous atmospheres: RRTM, a validated correlated-k model for the longwave. *Journal of Geophysical Research: Atmospheres*, 102 (D14), 16663-16682.

Myneni, R.B., Hoffman, S., Knyazikhin, Y., Privette, J.L., Glassy, J. *et al.,* 2002. Global products of vegetation leaf area and fraction absorbed PAR from year one of MODIS data. *Remote Sensing of Environment*, 83 (1), 214-231.

Papadopoulos, A., Katsafados, P., 2009. Verification of operational weather forecasts from the POSEIDON system across Eastern Mediterranean. *Natural Hazards and Earth System Sciences*, 9 (4), 1299-1306.

Papadopoulos, A., Korres, G., Katsafados, P., Ballas, D., Perivoliotis, L. *et al.,* 2011. Dynamic downscaling of the ERA-40 data using a mesoscale meteorological model. *Mediterranean Marine Science*, 12 (1), 183-198.

Powers, J.G., Klemp, J.B., Skamarock, W.C., Davis, C.A., Dudhia, J. *et al.,* 2017. The weather research and forecasting model: Overview, system efforts, and future directions. *Bulletin of the American Meteorological Society*, 98, 1717-1737.

Ricchi, A., Miglietta, M.M., Barbariol, F., Benetazzo, A., Bergamasco, A. *et al.,* 2017. Sensitivity of a Mediterranean

tropical-like cyclone to different model configurations and coupling strategies. *Atmosphere*, 8 (5), 92.

Ricchi, A., Miglietta, M.M., Bonaldo, D., Cioni, G., Rizza, U. *et al*., 2019. Multi-physics ensemble versus Atmosphere-Ocean coupled model simulations for a tropical-like cyclone in the Mediterranean Sea. *Atmosphere*, 10 (4), 202.

Rizza, U., Canepa, E., Ricchi, A., Bonaldo, D., Carniel, S. *et al.,* 2018. Influence of wave state and sea spray on the roughness length: Feedback on medicanes. *Atmosphere*, 9 (8), 301.

Rutgersson, A., Nilsson, E.O., Kumar, R., 2012. Introducing surface waves in a coupled wave-atmosphere regional climate model: Impact on atmospheric mixing length. *Journal of Geophysical Research: Oceans*, 117 (C11).

Shimada, S., Ohsawa, T., 2011. Accuracy and characteristics of offshore wind speeds simulated by WRF. *Sola*, 7, 21-24.

Sikirić, M.D., Roland, A., Janeković, I., Tomažić, I., Kuzmić, M., 2013. Coupling of the Regional Ocean Modeling System (ROMS) and Wind Wave Model. *Ocean Modelling*, 72, 59-73.

Skamarock, W.C., Klemp, J.B., Dudhia, J., Gill, D.O., Barker, D.M. *et al.,* 2008. *A description of the advanced research WRF Ver. 3.0*. NCAR Technical Note, Boulder, Colorado, USA, 125 pp. (Online available at: http://www2.mmm.ucar.edu/wrf/users/docs/arw_v3.pdf, accessed 19.11.2018)

Soukissian, T., Denaxa, D., Karathanasi, F., Prospathopoulos, A., Sarantakos, K. *et al.,* 2017. Marine renewable energy in the Mediterranean Sea: status and perspectives. *Energies,* 10 (10), 1512.

Staneva, J., Wahle, K., Günther, H., Stanev, E., 2016. Coupling of wave and circulation models in coastal-ocean predicting systems: a case study for the German Bight. *Ocean Science*, 12 (3), 797-806.

Strajnar, B., Cedilnik, J., Fettich, A., Ličer, M., Pristov, N. *et al.,* 2019. Impact of two-way coupling and sea-surface temperature on precipitation forecasts in regional atmosphere and ocean models. *Quarterly Journal of the Royal Meteorological Society*, 145 (718), 228-242.

Sullivan, P.P., Edson, J.B., Hristov, T., McWilliams, J.C., 2008. Large-eddy simulations and observations of atmospheric marine boundary layers above nonequilibrium surface waves. *Journal of the Atmospheric Sciences*, 65 (4), 1225-1245.

Taylor, K.E., 2001. Summarizing multiple aspects of model performance in a single diagram. *Journal of Geophysical Research: Atmospheres*, 106 (D7), 7183-7192.

Tewari, M., Chen, F., Wang, W., Dudhia, J., LeMone, M.A. *et al.,* 2004. Implementation and verification of the unified NOAH land surface model in the WRF model. p. 2165-2170. In: *20th Conference on Weather Analysis and Forecasting/16th Conference on Numerical Weather Prediction, 12-16 January 2004*. American Meteorological Society, Seattle, USA,

Thompson, G., Field, P. R., Rasmussen, R. M., Hall, W. D., 2008. Explicit forecasts of winter precipitation using an improved bulk microphysics scheme. Part II: Implementation of a new snow parameterization. *Monthly Weather Review*, 136 (12), 5095-5115.

Thompson, G., Tewari, M., Ikeda, K., Tessendorf, S., Weeks, C. *et al.,* 2016. Explicitly-coupled cloud physics and radiation parameterizations and subsequent evaluation in WRF high-resolution convective forecasts. *Atmospheric Research*, 168, 92-104.

Tucker, M.J., Pitt, E.G., 2001. *Waves in ocean engineering. Vol. 5.* Elsevier Science, New York, USA, 548 pp.

Valcke, S., Craig, T., Coquart, L., 2015. *OASIS3-MCT_3.0 coupler User Guide*. CERFACS/CNRS, Toulouse, France, 58 pp. (Online available at: http://www.cerfacs.fr/oa4web/oasis3-mct_3.0/oasis3mct_UserGuide.pdf, accessed 19.11.2018)

Varlas, G., 2017. *Development of an integrated modeling system for simulating the air-ocean wave interactions*. PhD Dissertation, Department of Geography, Harokopio University, Athens, Greece, 212 pp. (Online available at: https://www.didaktorika.gr/eadd/handle/10442/41238, accessed 19.11.2018)

Varlas, G., Anagnostou, M., Spyrou, C., Papadopoulos, A., Kalogiros, J. *et al.,* 2019a. A Multi-Platform Hydrometeorological Analysis of the Flash Flood Event of 15 November 2017 in Attica, Greece. *Remote Sensing*, 11 (1), 45.

Varlas, G., Katsafados, P., Korres, G., Papadopoulos, A., 2019b. Assessing the impact of Argo floats temperature measurements on the numerical weather prediction forecast skill. *Mediterranean Marine Science*, 20 (2), 331-341.

Varlas, G., Katsafados, P., Papadopoulos, A., Korres, G., 2018. Implementation of a two-way coupled atmosphere-ocean wave modeling system for assessing air-sea interaction over the Mediterranean Sea. *Atmospheric Research*, 208, 201-217.

Varlas, G., Papadopoulos, A., Katsafados, P., 2019c. An analysis of the synoptic and dynamical characteristics of hurricane Sandy (2012). *Meteorology and Atmospheric Physics*, 131 (3), 443-453.

Voldoire, A., Sanchez-Gomez, E., Salas y Mélia, D., Decharme, B., Cassou, C. *et al.,* 2013. The CNRM-CM5. 1 global climate model: description and basic evaluation. *Climate Dynamics*, 40 (9-10), 2091-2121.

Wahle, K., Staneva, J., Koch, W., Fenoglio-Marc, L., Ho-Hagemann, H. *et al.,* 2017. An atmosphere-wave regional coupled model: improving predictions of wave heights and surface winds in the southern North Sea. *Ocean Science*, 13 (2), 289-301.

WAMDI group: Hasselmann, S., Hasselmann, K., Bauer, E., Janssen, P.A.E.M., Komen, G.J. *et al.,* 1988. The WAM model - a third generation ocean wave prediction model. *Journal of Physical Oceanography*, 18, 1775-1810.

Wilks, D.S., 2011. *Statistical methods in the atmospheric sciences*. *Vol. 100*. Academic press, Oxford, UK, 704 pp.

Wu, J., 1982. Wind-stress coefficients over sea surface from breeze to hurricane. *Journal of Geophysical Research: Oceans*, 87(C12), 9704-9706.

Zhang, J.A., Black, P.G., French, J.R., Drennan, W.M., 2008. First direct measurements of enthalpy flux in the hurricane boundary layer: The CBLAST results. *Geophysical Research Letters*, 35 (14).